

Article

Non-Intrusive Voltage-Inversion Measurement Method for Overhead Transmission Lines Based on Near-End Electric-Field Integration

Wei Liao ¹, Qing Yang ^{1,*}, Kun Ke ¹, Zhenhui Qiu ¹, Yuqing Lei ² and Fei Jiao ²

¹ State Key Laboratory of Power Transmission Equipment and System Security and New Technology, Chongqing University, Chongqing 400044, China; 202011021056t@cqu.edu.cn (W.L.)

² China Electric Power Research Institute, Beijing 100192, China

* Correspondence: yangqing@cqu.edu.cn

Abstract: Existing electric-field integral inversion methods have limited field application conditions, and they are difficult to arrange electric-field measurement points on high-span overhead lines. This paper proposes a non-intrusive voltage measurement method for overhead transmission lines based on the near-end electric-field integration method. First, the electric-field distribution under 10 kV lines is calculated by finite element simulation software. The electric-field distribution of the plumb line and the discrete integral node below the wire are analyzed. Then, based on traditional electric-field integration, a line-voltage-inversion measurement method based on near-end electric-field integration is proposed. In addition, a voltage-monitoring system based on near-end electric-field integration is constructed. Next, the numerical integration types, the number of integration nodes, and the scale coefficient of the near-end region of the inversion algorithm are optimized with the electric-field simulation data. Finally, to verify the voltage-inversion method proposed in this paper, a test platform for overhead-line voltage is constructed using a MEMS electric-field sensor. The results indicate that the voltage-inversion error is 5.75%. The research results will provide theoretical guidance for non-intrusive voltage-inversion measurement of overhead lines.

Keywords: overhead line; electric-field integration method; non-intrusive voltage measurement; voltage-inversion measurement



Citation: Liao, W.; Yang, Q.; Ke, K.; Qiu, Z.; Lei, Y.; Jiao, F. Non-Intrusive Voltage-Inversion Measurement Method for Overhead Transmission Lines Based on Near-End Electric-Field Integration. *Energies* **2023**, *16*, 3415. <https://doi.org/10.3390/en16083415>

Academic Editor: Nicu Bizon

Received: 15 March 2023

Revised: 3 April 2023

Accepted: 11 April 2023

Published: 13 April 2023



Copyright: © 2023 by the authors. Licensee MDPI, Basel, Switzerland. This article is an open access article distributed under the terms and conditions of the Creative Commons Attribution (CC BY) license (<https://creativecommons.org/licenses/by/4.0/>).

1. Introduction

A strong and reliable smart grid is the future development trend of the power grid, and it is significant to improve the holographic sensing ability of power links for the construction of a smart grid [1–3]. Voltage is one of the most important electric parameters to be monitored in power systems. Obtaining massive voltage data of power systems safely, accurately, and without interference can guarantee the safety protection and stable operation of the system [4]. The non-intrusive voltage measurement technique does not require a direct electrical connection to the line or equipment, and it can accurately measure voltage and avoid interference with the system to be measured. Non-intrusive voltage measurement technology meets the requirements of sensing technology in smart grids [5–7]. At present, small- and microelectric-field sensors such as the micro-electro-mechanical system (MEMS) electric-field sensor [8,9], optical electric-field sensor [10,11], and D-dot electric-field sensor [12,13] can accurately measure the spatial electric-field distribution around the conductor. The microelectric-field sensor combined with the voltage-inversion algorithm can realize the non-intrusive inversion measurement of line voltage. Compared with existing non-intrusive voltage sensors based on stray capacitance–voltage division [14,15] or electric-field coupling principle [16,17], it avoids the problem that stray electricity is susceptible to the environment. Microelectric-field sensor technology has developed rapidly in

recent years [18,19], which provides a reliable device basis for realizing voltage inversion. Therefore, it has been widely concerned by researchers.

According to the principle of inversion measurement, existing non-intrusive voltage measurement methods are mainly divided into the electric-field inverse problem-solving method [20,21] and the electric-field integration method. When the shape of the wire is known, the voltage of the wire can be easily measured by fixing the electric-field-measuring point around the wire. This method is commonly used to monitor transient voltage of wire. This method will cause phase error when measuring steady-state voltage in multi-conductor environment. The voltage-inversion method based on the inverse problem of the electric field realizes voltage calculation by establishing an inverse solution model of the field to the source; however, this voltage-inversion method involves complex matrix inverse operations, so it is not suitable for real-time voltage measurement. The electric-field integration method calculates the potential difference between the conductor and the zero-potential point by the discrete numerical integration method to realize accurate voltage measurement. The electric-field integration method was first used in distributed optical voltage transformers [22,23]. Chavez employed a small optical field sensor to measure three-point electric-field information in a dielectric shielding cavity [24]. The electric-field integral value of the vertical line between the high-voltage electrode and the ground electrode is calculated by a numerical integration method. This optical voltage transformer can non-intrusively measure the busbar voltage. Jingang Wang et al. [25] proposed to apply the electric-field integration method to the voltage-monitoring of transmission lines. By placing multiple D-dot electric-field sensors on the plumb line between the transmission line and the ground, they accurately measured the voltage of the line combined with the electric-field integration method. Additionally, Jingang Wang [26] also proposed a Gauss integration algorithm with fixed nodes to optimize the placement of electric-field sensors. The existing electric-field integration method avoids the complex and ill-conditioned issues of the inverse problem-solving method; however, it needs to arrange multiple electric-field sensors on the plumb line below the transmission line. Due to the large height of the actual overhead line, it is almost impossible to suspend several electric-field sensors directly below the line. Moreover, the remote arrangement between the electric-field sensors also brings challenges to the synchronous communication between the sensors. At present, the voltage-inversion measurement method based on the principle of electric-field integration has been verified to have high accuracy in 230 kV optical voltage transformer; however, there are few researches on the application of the electric-field integration method to the voltage measurement of overhead lines. At present, only the verification test is carried out in the laboratory, and the highest measured line voltage reaches 20 kV. This method, although theoretically excellent, has not been applied to other higher voltage levels. The reason is that the existing methods do not fully consider the difficulty of practical application, and the actual implementation is difficult.

In general, environmental stray capacitance can easily interfere with the existing contactless voltage measurement methods by capacitive coupling, and so the actual measurement accuracy is often low; however, the method of calibrating wire voltage by measuring the electric field of a single point has the defect of phase error in the multi-conductor environment. The method of voltage inversion by measuring the electric field of multiple points has high accuracy in theory; however, the existing methods have high requirements for sensor layout and communication, so it is difficult to measure in practice. Therefore, it is necessary to study the further modification method of electric-field integration method. If the line voltage can be inversely measured by placing sensors near the wire, the feasibility of the field integration method will be further improved.

Based on the traditional electric-field integration method, this paper proposes a line-voltage inversion measurement method based on near-end electric-field integration. Firstly, the measurement principle of conventional electric-field integration is analyzed. Then, the electric-field distribution on the plumb line below the conductor is calculated by finite element simulation software. The waveforms of electric-field intensity at different positions

of integral nodes are calculated. In addition, the distribution law of the electric field along the plumb line and the problem of electric-field coupling interference are analyzed. Based on these analyses, a voltage inversion calculation method based on near-end electric-field integration is proposed. Next, according to the near-end integration method, the voltage-monitoring device and the system scheme of the overhead transmission line are proposed. Based on the finite simulation data, the scale coefficient of the near-end region, the type of the integration algorithm, and the number of integration nodes are optimized. Finally, an experimental platform for voltage-inversion measurement of high-voltage overhead lines is constructed to test and verify the voltage-inversion method proposed in this paper.

2. The Measurement Principle of the Near-End Electric-Field Integral Method

2.1. Electric-Field Integration Method

The spatial electric field generated by the steady-state voltage of the overhead line is a quasi-static field, and it has the property of an electrostatic field. According to the definition of the potential at a point in space in the electrostatic field, the potential at a point is equal to the work done by the force of the electric field by moving the unit positive charge from the point to infinity. Thus, the wire potential φ can be expressed as:

$$\varphi = \int_p^{\infty} \vec{E} \cdot d\vec{l} \quad (1)$$

where \vec{E} is the electric field experienced by a unit charge as it moves. \vec{l} is the path of charge movement. The electric-field vector \vec{E} is positive in the vertical downward direction. The distance vector \vec{l} is positive vertically upward. Then, the potential difference U_{ba} between any two points in the electrostatic field is the work done by the unit positive charge moving from point a to point b along any line. The potential difference U_{ba} can be expressed as:

$$U_{ba} = \int_b^a \vec{E} \cdot d\vec{l} = \int_b^{\infty} \vec{E} \cdot d\vec{l} - \int_a^{\infty} \vec{E} \cdot d\vec{l} \quad (2)$$

Figure 1 shows the voltage measurement model for overhead transmission lines based on the electric-field integration method. Where the height of the wire is H m. The potential of the ground is assumed to be 0 V. According to Formula (2), the voltage of the wire U is:

$$U = - \int_0^H \vec{E} \cdot d\vec{l} \quad (3)$$

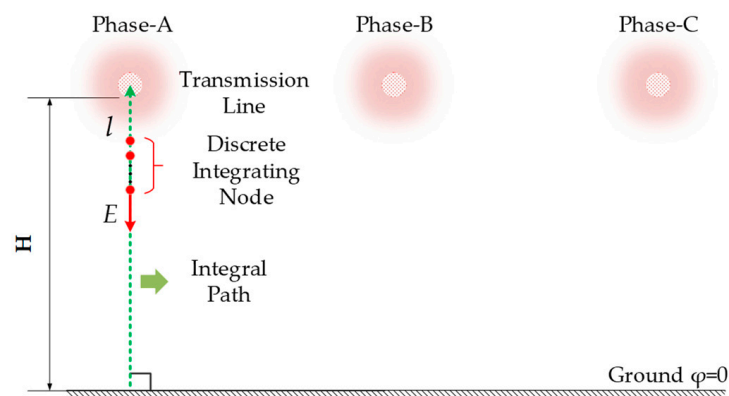


Figure 1. The voltage measurement model for overhead transmission lines based on the electric-field integration method.

To facilitate calculation, the plumb line of traverse and ground is taken as the integral path. According to the calculation principle of discrete numerical integration, the definite

integral value on the finite region can be converted to the sum of the product of the function value at the integral node and the corresponding proportionality coefficient. Therefore, line voltage U can be calculated by:

$$U \approx \sum_{k=1}^n \alpha_k E(x_k) \quad (4)$$

where α_k is the integral weight, x_k is the position of the integrating node, $E(x_k)$ is the electric-field intensity on the integrating node, and n is the number of integrating nodes. Note that although the discrete integral method makes line-voltage and wire-height factors unrelated formally, the integral weight and the electric-field strength are directly related to the line height.

2.2. Analysis of Electric-Field Distribution of Plumb Line below the Line

The electric-field integral inversion method realizes voltage inversion based on the electric-field distribution of the plumb line below the conductor. To improve the existing integral inversion method, it is necessary to analyze the spatial electric-field distribution of overhead lines. In this study, the COMSOL Multiphysics finite element simulation software is used to calculate the electric-field distribution rule below the line. In the simulation model, the three-phase lines are arranged horizontally. The wire material is set to aluminum, and the radius and length of the wire are set to 16 mm and 2 m, respectively. The distance between the conductor and the ground is 6.5 m, and the distance between the adjacent phase conductors is 0.65 m. The wire voltage is set to 10 kV three-phase voltage with a voltage frequency of 50 Hz. The ground boundary voltage is set to 0 V. A line segment from the ground to the surface of the wire is set directly below the central position of the line as the observation calculation path. In the finite element simulation, the cross section is first partitioned using a free triangular mesh. Then the overall 3D model is meshed by sweeping. The settings of the free triangular mesh division include: the maximum cell size is set to 0.15 m, the minimum cell is set to 0.02 m, the maximum cell growth rate is 1.08, and the curvature factor is 0.35. The cross-sectional view of the mesh division is shown in Figure 2 below.

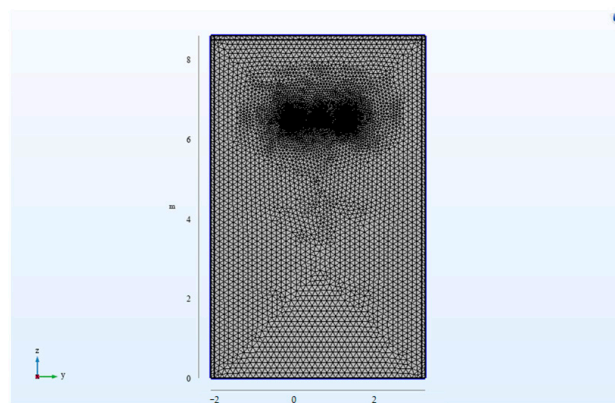


Figure 2. The cross-sectional view of the mesh division.

The electric-field distribution of the plumb line below the three-phase conductor is calculated. The analysis of the electric field below the A-phase wire is taken as an example. When $t = 0.05$ s, the electric-field distribution of the plumb line below the A-phase wire is shown in Figure 3. Where the vertical coordinate E is the electric-field strength in the vertical ground direction, the horizontal coordinate h is the vertical height from the ground.

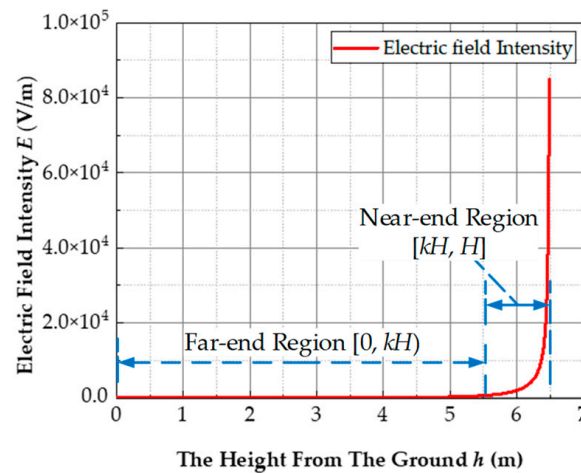


Figure 3. The electric-field distribution below the A-phase wire.

It can be seen from Figure 3 that the electric-field intensity in the near-end integration region near the line is strong. As the distance r from the wire increases, the intensity of the electric field decreases sharply. The electric-field intensity in the far-end region away from the overhead line is weak, and it decreases very slowly as the distance r from the wire increases. According to the above electric-field distribution characteristics, the plumb line below the wire can be divided into the near-end region and the far-end region. The proportion coefficient of the near-end integral region is denoted as k , and the vertical height of the line from the ground is denoted as H m. The plumb line below the conductor is divided according to the height x from the ground. When $x \in [0, kH]$, it is a far-end region, and when $x \in [kH, H]$, it is a near-end region. When $x = kH$ m, this point belongs to the near-end region. According to the definition of potential, the wire voltage can be equivalent to the area formed by the curve and the horizontal axis in Figure 3. From the electric-field distribution of the plumb line below the wire in Figure 3, it can be seen that the integral area of the near-end area is almost close to the integral area of the whole curve.

The choice of integration node is one of the key factors affecting the accuracy of the electric-field integration method. It is necessary to analyze the electric-field waveform at different points on the plumb line below the wire. Taking the A-phase wire as an example, the electric-field intensity at multiple nodes in the near-end and far-end regions below the 10 kV wire is simulated, with the height of the integrating node set to $h = 6.3$ m, 6.0 m, 5.0 m, 2.0 m, respectively.

Figure 4 shows the electric-field variation curves of integration nodes at different positions below the A-phase conductor of the 10 kV line. The results indicate that the amplitude of the electric-field intensity decreases with the decrease in the node height. The integration nodes at $h = 6.3$ m and $h = 6.0$ m belong to the near-end region. Its electric-field intensity waveform amplitude is strong, and the phase difference between the electric-field intensity and the wire voltage is small. The integration nodes at $h = 5.0$ m and $h = 2.0$ m belong to the far-end region. The amplitude of the electric-field intensity waveform of the node in the far-end region is small; the phase difference between electric the field intensity and the wire voltage is large. According to Formula (4), the existence of such phase difference will directly bring a phase error to the inversion line voltage. Where the vertical coordinate E is the electric-field strength in the vertical ground direction at the calculated node. The horizontal coordinate t is the time of the electric-field waveform, and here two sine periods are chosen.

The reason for the phase difference is that other phase conductors will produce an interference electric field below the conductor to be measured. Since the integration nodes in the near-end region are very close to the conductor to be measured, their electric-field intensity mainly comes from the strong electric field of the conductor to be measured. Additionally, according to the electric-field distribution law in Figure 4, the electric field of

the coupling interference generated by other phase conductors will attenuate very little due to the existence of large phase spacing. As the height of the integration node decreases, the electric field from the conductor under test will be significantly attenuated, and the phase difference increases gradually due to the interference electric field of the adjacent phase conductor. Based on the above analysis, it is obvious that selecting the integration node in the near-end region not only facilitates the layout of sensors but also effectively reduces the interference generated by adjacent phase conductors.

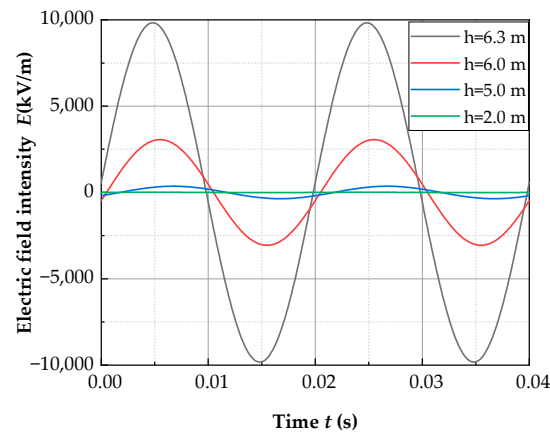


Figure 4. The electric-field variation curves of the integration nodes at different positions below the A-phase conductor of the 10 kV line.

2.3. The Principle of the Near-End Electric-Field Integral Method

Because the electric field around the wire is concentrated around the wire, the area formed by the near-end region and the horizontal axis is much larger than that formed by the far-end region and the horizontal axis. So, if the near-end region coefficient k is selected reasonably, the transmission-line voltage can be accurately calculated by the electric-field integration method. Meanwhile, the integral node is near the wire when integral inversion is carried out for the near-end area. This means that the field sensors need to be only placed near the wires. With this method, the difficulty of sensor installation in the traditional electric-field integration method is effectively overcome, and the accuracy of voltage calculation can be also guaranteed. According to the above analysis, the calculation formula of transmission-line voltage U based on the near-end electric-field integration method can be expressed as:

$$U = \int_0^{kH} E(x)dx + \int_{kH}^H E(x)dx \approx \int_{kH}^H E(x)dx = \sum_{i=1}^N \alpha_i E(x_i) + R[f] \approx \sum_{i=1}^N \alpha_i E(x_i) \quad (5)$$

where α_i and x_i are the integral weight and the position of the integration node in the near-end area, respectively. $E(x_i)$ is the electric-field intensity at the integrating node in the near-end region. N is the number of integrating nodes. $R[f]$ is the error remainder brought by the discrete numerical integration method, and it is related to the type of the numerical integration method, the number of integrating nodes, the proportion coefficient of the near-end region, and other factors.

In Formula (5), the electric-field integral x_i and the integral weight α_i need to be calculated by the numerical integration method. The Gauss-type integral method is a numerical integration method with an algebraic precision of $2n + 1$, and it has been proven to have good accuracy in the traditional voltage inversion algorithm based on electric-field integration. In this study, two integral methods, Gauss–Legendre integral and Gauss–Chebyshev integral, are adopted to calculate the integral node x_i and the integral weight α_i .

(1) Gauss–Legendre integral

When the weighted function $\rho(x) = 1$ and the integration interval are normalized, the zero point of the Legendre polynomial is the Gaussian integral node x_i , where the position of the integral node satisfies:

$$\begin{aligned} P_0(x) &= 1 \\ P_j(x) &= \frac{1}{2^j n!} \frac{d^j}{dx^j} [(x^2 - 1)^j] \quad (j = 1, 2, \dots, n) \end{aligned} \quad (6)$$

where $P_j(x)$ is the j th Legendre polynomial, and n is the number of integrating nodes. According to the definition of algebraic precision of the integral formula, when the integral formula holds for any $f(x) = x^m$, ($m = 0, 1, 2, \dots, 2n + 1$), it has an algebraic precision of $2n + 1$. The integral weight α_k ($k = 0, 1, \dots, n$) can be obtained by substituting the position of the integral node x_k ($k = 0, 1, \dots, n$) into Formula (4):

$$\begin{bmatrix} x_0^0 & x_1^0 & \cdots & x_n^0 \\ x_0^1 & x_1^1 & \cdots & x_n^1 \\ \vdots & \vdots & \ddots & \vdots \\ x_0^{2n+1} & x_1^{2n+1} & \cdots & x_n^{2n+1} \end{bmatrix} \begin{bmatrix} \alpha_0 \\ \alpha_1 \\ \vdots \\ \alpha_n \end{bmatrix} = \begin{bmatrix} \int_a^b x^1 dx \\ \int_a^b x^2 dx \\ \vdots \\ \int_a^b x^n dx \end{bmatrix} \quad (7)$$

(2) Gauss–Chebyshev integral

When the weighted function $\rho(x) = 1/(1 - x^2)^{1/2}$ and the interval are normalized, the zero point of the Chebyshev polynomial is the Gaussian point x_i , where the position of the integral node satisfies:

$$x_i = \cos \left[\frac{2i + 1}{2\pi(n + 1)} \right] \quad (8)$$

where $i = 1, 2 \dots n$, and n is the number of integrating nodes.

The integral weight calculation formula is:

$$\alpha_n = \frac{(1 - k)H}{n} \quad (9)$$

where k is the scale coefficient of the near-end integral region, and H is the vertical height of the line from the ground.

The error source of the voltage-inversion algorithm based on the near-end electric-field integral is denoted as the error residual term $R[f]$. The size of the error residual term is related to the numerical integration method, the number of numerical integration nodes, and the scale coefficient k of the near-end region. The following optimization is conducted for the factors affecting the accuracy of these algorithms.

The flow chart of the line-voltage inversion algorithm based on the near-end electric-field integration method is shown in the Figure 5. After determining the parameters such as the alignment shape and height of the conductor, the algorithm parameters such as the scale factor of the near-end region, the number of integration nodes, and the type of numerical integration are optimally selected. Then the integration node positions and the integration weights are calculated according to the determined algorithm parameters. The device is designed to install the MEMS electric-field sensor at the corresponding position according to the above algorithm solution results. Then, the voltage of the wire is accurately calculated by the electric-field measurement data and the voltage-inversion algorithm. It should be noted that we performed simulated calculations when optimizing the parameters of the algorithm. The electric-field data used in the simulated calculations were obtained by finite element simulation. In the validation tests, the electric-field data were obtained by MEMS electric-field sensor measurements.

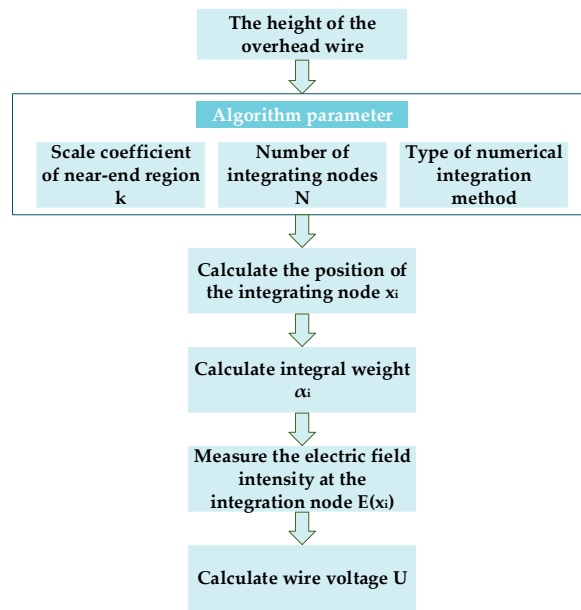


Figure 5. The flow chart of the line-voltage inversion algorithm.

2.4. Scheme of the Measurement System

The online monitoring of transmission-line voltage can be realized by combining the near-end electric-field integration method and the MEMS electric field. The overhead-line-voltage monitoring system based on the near-end electric-field integration method is shown in Figure 6. The system consists of a non-intrusive voltage-measuring device and an upper monitoring computer. The non-intrusive voltage-measuring devices are designed according to the near-end electric-field integration theory. Inside the device are multiple arrays of microelectric-field sensors. The electric-field sensor array can accurately measure the electric-field intensity at the desired integration node. The voltage-measuring device includes a high-speed data acquisition unit (DAU), a narrowband internet of things (NBIOT) module, and a microcontrol unit (MCU). The DAU and MCU can collect the electric-field data of each node and calculate the wire voltage internally. Meanwhile, the NBIOT module sends the voltage-monitoring data to the upper computer. This scheme effectively addresses the issue that the existing electric-field integration method is difficult to apply to the transmission line.

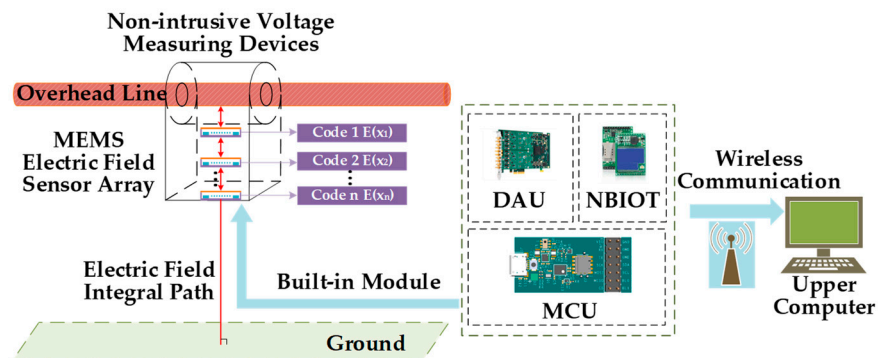


Figure 6. The overhead-line-voltage monitoring system based on the near-end electric-field integration method.

The near-end electric-field integration method calculates voltage through the electric-field data of the discrete integration node. Therefore, it is crucial to accurately measure the electric-field intensity at the integration node. Due to the limited space inside the device, the size and power consumption of the sensor need to be low enough; however, the existing

advanced microelectric-field sensor technology provides a solution to this problem. In this paper, a MEMS electric-field sensor is exploited to measure the electric field at the node. The image of the MEMS electric-field sensor used in this study and the microstructure of the internal MEMS chip are shown in Figure 7, where the yellow one is the packaged MEMS electric-field sensor and the part pointed by the white arrow is the microstructure of the internal MEMS chip. Encapsulated MEMS electric-field sensors are insensitive to meteorological and environmental factors and have been used for atmospheric electric-field measurements at high altitudes [27]. The sensor adopts a MEMS chip of field grinding electric-field sensor, which is encapsulated by ceramic material. The measurement range of the MEMS is higher than ± 100 kV/m, the resolution is up to 15 V/m, and the accuracy is higher than 2%. The sensor is powered by a ± 5 V DC power supply.

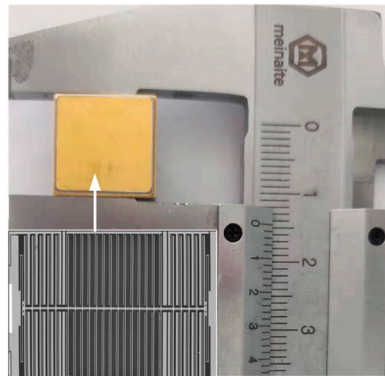


Figure 7. The MEMS electric-field sensor and the internal MEMS-chip microstructure.

3. Optimization of Near-End Electric-Field Integration Algorithm

3.1. Numerical Integration Type and Node Number Optimization

Firstly, the scale coefficient of the near-end integral interval is temporarily set to 0.9. The different numerical integration method is used to calculate the location of the integration node in the near-end region. In finite element simulation, the electric-field information of each point on the plumb line below the three-phase line is extracted and substituted into the near-end integral inversion algorithm. The relative errors of inversion three-phase voltage's amplitude obtained by the inversion of the two integration algorithms and different numbers of nodes in the near-end interval are shown in Table 1. The calculation formula for relative errors of inversion three-phase voltage's amplitude is as follows:

$$\varepsilon_{r-X} = \frac{U_{inver-X} - U_{actual-X}}{U_{actual-X}} (X = A, B, C) \quad (10)$$

where ε_{r-A} , ε_{r-B} and ε_{r-C} are relative errors of A-, B- and C-phase inversion voltage's amplitude respectively. $U_{inver-X}$ is amplitude of inversion voltage for phase A, B or C. $U_{actual-X}$ is amplitude of actual voltage for phase A, B or C.

The results in Table 1 indicate that for the same integration method, the relative errors of inversion voltage's amplitude decrease gradually with the increase in the number of integration nodes. In addition, the Gauss–Chebyshev integral method is more accurate than Gauss–Legendre integral method. When the number of integrating nodes is 2 to 5, the relative errors of the Gauss–Chebyshev integral method are all less than 10%, while the relative errors of the Gauss–Legendre integral method are all more than 10%. Furthermore, it can be seen from the table that the Gauss–Chebyshev integral method converges faster than the Gauss–Legendre integral method. The former can achieve higher precision inversion with fewer integration nodes. The fewer the number of integration nodes, the fewer the number of sensors placed near the line, the simpler the internal layout of the measurement system, and the lower the cost. Therefore, as few integral nodes should be selected as possible on the premise of ensuring measurement accuracy. According to the calculation results of the

Gauss–Chebyshev integral method with different numbers of integrating nodes, when the number of nodes is three, the relative errors of inversion three-phase voltage’s amplitude is small. Therefore, this study finally chooses the three-point Gauss–Chebyshev integral method as the best scheme for the near-end voltage inversion of 10 kV lines.

Table 1. The relative error of inversion voltage’s amplitude with different numerical integration methods and numbers of nodes.

Integral Method	The Number of Integration Nodes N	ε_{r-A}	ε_{r-B}	ε_{r-C}
Gauss–Legendre Integral	2	−43.21%	−41.33%	−43.47%
	3	−37.17%	−34.10%	−37.37%
	4	−24.17%	−20.56%	−24.33%
	5	−17.32%	−13.28%	−17.51%
Gauss–Chebyshev Integral	2	−9.11%	−2.68%	−9.47%
	3	−2.25%	2.56%	−2.55%
	4	−2.09%	2.89%	−2.22%
	5	−2.01%	3.78%	−1.97%

3.2. Optimization of the Near-End Region Coefficient k

The near-end electric-field integral method mainly calculates the electric-field integral value in the near-end area of the wire. Therefore, it is crucial to select the proportional coefficient of the near-end integral region reasonably to improve the measurement accuracy. According to the optimization results in Section 3.1, three integration nodes are selected in the near-end region and calculated by the Gauss–Chebyshev integral method. Considering that the scale coefficient of the near-end region falls within $[0.75, 0.95]$, the inversion voltage under different k values is calculated.

Figure 8 shows the variation law of maximum relative error of the three-phase voltage’s amplitude ε_{rmax} with respect to the k value. The calculation formula for ε_{rmax} is as follows:

$$\varepsilon_{rmax} = \max\{|\varepsilon_{r-A}|, |\varepsilon_{r-B}|, |\varepsilon_{r-C}|\} \quad (11)$$

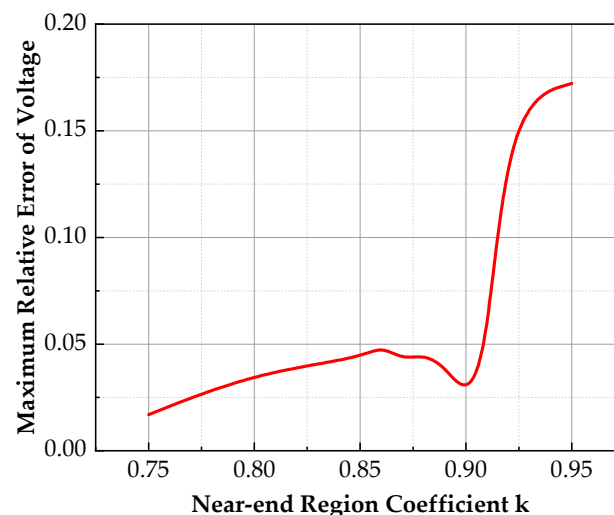


Figure 8. The influence law of the near-end integral region coefficient on the maximum relative error of the inversion voltage.

The results in Figure 8 indicate that when the k value starts to decrease, the relative error of the maximum value of the inversion three-phase voltage decreases rapidly; then, it stops decreasing and rises slightly around $k = 0.9$; finally, it continues to decline slowly after $k = 0.86$ and reaches the minimum value at $k = 0.9$. When $k \in [0.9, 0.95]$, the near-end

region is too small, and a large remaining integral area is ignored, resulting in a large error. As k decreases, the near-end integral region expands. The remaining integral area to be ignored decreases, so the error decreases. When $k \in [0.86, 0.9)$, the near-end region is almost close to the whole integral of the curve; however, since the integral node is far away from the conductor, the proportion of interference components generated by adjacent phase conductors increases, so the error increases slowly. When $k \in [0.75, 0.86)$, because the integration nodes are far away from the conductor, the interference proportion of other phases do not change significantly; however, as the near-end integral area continues to expand, the measurement error decreases slowly as the near-end integral area increases.

When selecting the near-end integration region coefficient, it should be ensured that the near-end integration area is large and the integration node can be close to the charged conductor. Although the inversion error is smaller when $k \leq 0.75$, the unlimited reduction of k will inevitably bring about the decline of the integral node position. In this case, the near-end integration method will lose its meaning, and the problem of sensor layout will reappear. Therefore, $k = 0.9$ is finally selected in this study as the best near-end integral region coefficient of the three-point Gaussian-Chebyshev integral method for 10 kV transmission lines. According to the scheme, the three-phase voltage waveform obtained by the inversion is shown in Figure 9. The vertical coordinate U is the actual applied voltage or the inverse-calculated voltage of transmission line. The horizontal coordinate t is the time of the voltage waveform, and here two sine periods are chosen. The results indicate that the near-end integral inversion method proposed in this paper can achieve high-precision inversion calculation of overhead lines. The amplitude error and phase error of the three-phase voltage are small.

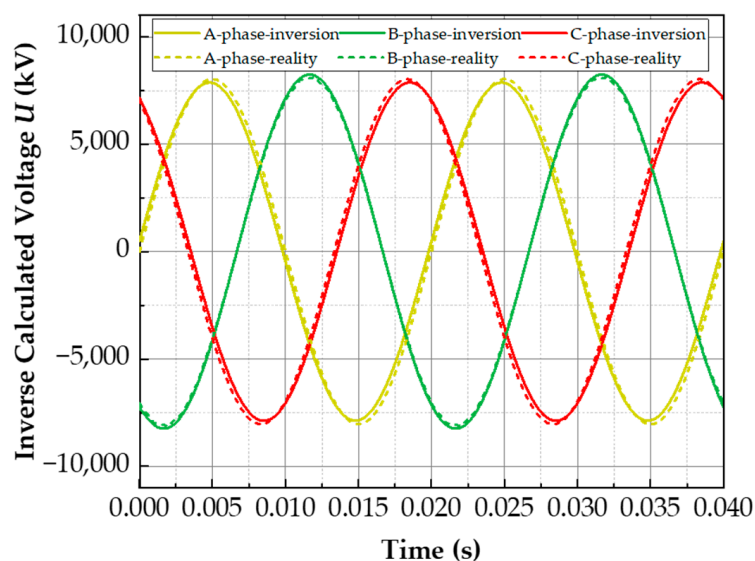


Figure 9. The results of three-point Gaussian–Chebyshev proximal integral inversion at $k = 0.9$.

4. Experimental Testing and Analysis

To verify the accuracy and feasibility of the voltage-inversion measurement method proposed in this paper, a non-intrusive voltage-inversion-measurement test platform for high-voltage overhead lines was built. The electric-field distribution below the wire was measured by a MEMS electric-field sensor. Meanwhile, a voltage-inversion algorithm is adopted to calculate the wire voltage and compare it with the actual voltage.

4.1. Construction of Experimental Platform

The non-intrusive voltage-measurement test platform of an overhead line was built, as shown in Figure 10. Power frequency AC signals are generated by an arbitrary waveform generator. The high-voltage amplifier amplifies the signal to produce a high-voltage

amplitude of 1×10^4 V onto the metal rod conductor. The diameter of the metal rod conductor is 16 mm, and the length is 3 m. The metal bar is supported to a certain height by two retractable insulating supports. The MEMS electric-field sensor is attached below the wire by a graduated plexiglass pillar, and it is used to measure the electric-field intensity below the wire. The height of the MEMS electric-field sensor is changed by adjusting the fixture. The actual voltage of the line is obtained by the capacitive voltage divider (the partial voltage ratio is 371:1) for comparison with the inversion voltage. Before the test, the position of the integration node of the corresponding proximal integral method has been calculated. The electric-field sensor is fixed at the corresponding position according to the calculated integral node position. Then, the voltage-inversion algorithm proposed in this paper is adopted to calculate wire voltage.

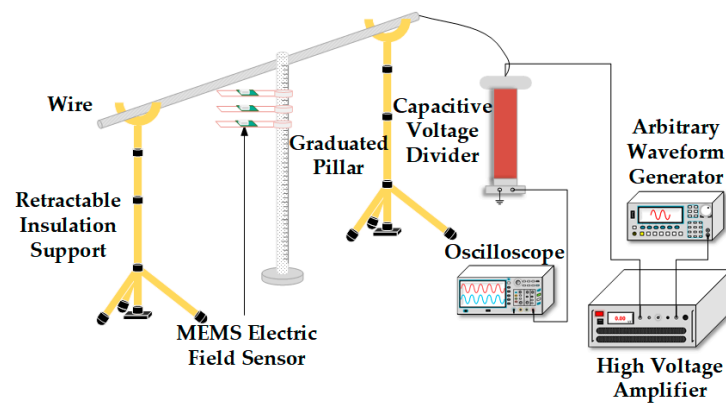


Figure 10. The non-intrusive voltage-measurement test platform for overhead lines.

4.2. Analysis of Experimental Results

Because the height of the actual overhead transmission line is 6 m~7 m, which is not suitable for laboratory testing, this paper measured the voltage of the wire with a height of 2 m. Since the height used in the test is lower than the actual one, the integral area proportion of the near-end area will decrease. Therefore, the scaling coefficient of the proximal region was set to 0.7, and the three-point Gauss Chebyshev integral method was used at the near end. The positions of each electric-field-measuring point are shown in Table 2, where x_1 , x_2 and x_3 are the heights of the three integrating nodes.

Table 2. The positions of the electric-field integral nodes during the test.

Region (m)	Node Position (m)
x_1	1.957
x_2	1.786
x_3	1.614

According to the calculated height information, the MEMS electric-field sensor is accurately arranged in the proximal integration area right below the wire, and it directly faces the wire so that the electric-field measured by the wire is in the plumb field direction. The electric-field waveform measured at three points near the end and calculated at the remote auxiliary node is shown in Figure 11. The vertical coordinate E is the electric-field intensity in vertical ground direction measured by MEMS electric-field sensor. The horizontal coordinates t are the time of the electric-field waveform, where two sine periods are recorded. The results indicate that the electric-field intensity of the measuring point on the plumb line decreases with the decrease in height.

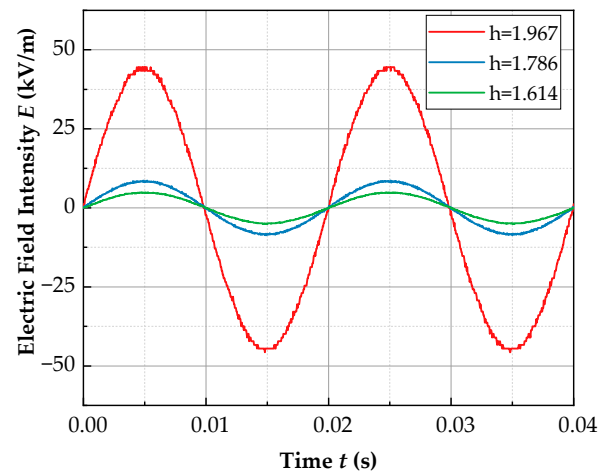


Figure 11. The electric-field waveform of three integral nodes measured by the MEMS electric-field sensor.

Then, the electric-field data measured above are substituted into the voltage-inversion algorithm to calculate the voltage of the line. Figure 12 presents the comparison between the voltage waveform calculated by the voltage-inversion algorithm and the actual line-voltage waveform. Where, U_a is the actual voltage of the wire, and U_i is the voltage obtained by inversion measurement. The comparison results indicate that the voltage waveform calculated by the voltage-inversion algorithm is almost consistent with the actual line-voltage waveform, and the amplitude error of the inversion voltage and the applied voltage is 5.75%. The analysis of the causes of error indicates that there are some errors in the MEMS electric-field sensor, the actual positioning position, and the theoretical height of the sensor. In addition, the electric-field sensor is secured by plexiglass pillars. The relative dielectric constant of plexiglass is about 2.3. Although the permittivity of plexiglass material is relatively small, it will distort the electric-field distribution in a small range. This is another reason for the discrepancy between measured and calculated values. The results of many tests show that the influence of the above error sources on the inversion is within an acceptable range. Since the height used in the experiment is much smaller than that of the actual overhead line, on the plumb line below the wire, the concentrated distribution of electric-field intensity in the near-end region is weakened. Therefore, if the measurement is made at a larger height, the error of the near-end integral method will be further reduced to close to the simulation calculation value. Finally, the experimental results verify the accuracy and feasibility of the proximal integral inversion method proposed in this paper.

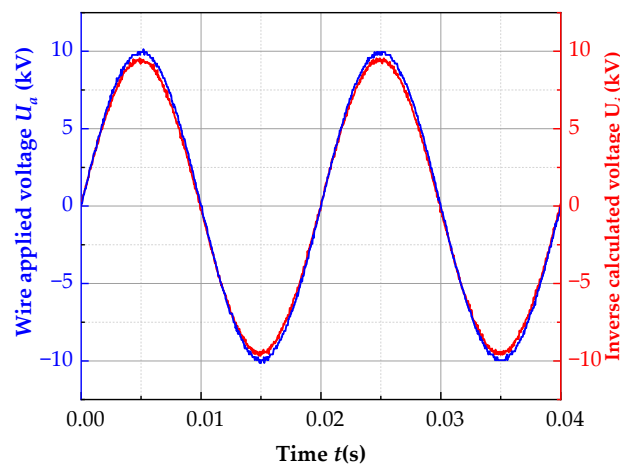


Figure 12. The inversion calculation of the line-voltage waveform and the actual voltage comparison.

5. Conclusions

Drawing on the traditional voltage measurement method, this paper proposes a voltage inversion method based on near-end electric-field integration:

- (1) The theoretical model of voltage inversion calculated by the electric-field integral method is established. The COMSOL Multiphysics finite element simulation software is employed to calculate the electric-field distribution under the 10 kV three-phase overhead line and the electric-field intensity waveform at different positions. The calculation results indicate that the electric-field intensity on the plumb line below the conductor is concentrated in the near-end region of the conductor, and the integration node in the near-end region is less affected by the electric-field crosstalk of the adjacent phase conductor. Then, a voltage-inversion algorithm based on the near-end electric-field integration method is proposed in this paper. Meanwhile, an overhead-line-voltage monitoring system is proposed based on the near-end electric-field integration method.
- (2) The voltage-inversion calculation is conducted by using the data of a finite simulated electric field, and the integration type, the number of integration nodes, the proportion coefficient of the proximal integration region, and the remote auxiliary nodes of the voltage-inversion algorithm are optimized. The results indicate that when $k = 0.9$, the three-point Gauss–Chebyshev integral method can realize accurate inversion of three-phase voltage, and the maximum error is 2.55%.
- (3) A test platform is built for voltage-inversion measurement of high-voltage overhead lines, and the electric-field waveform at each integral node below the line is measured through the MEMS electric-field sensor. The results indicate that when the ratio coefficient of the proximal region is $k = 0.7$, the error of voltage inversion by using the three-point Gauss–Chebyshev integral method and introducing a remote auxiliary node is 5.75%.

This paper provides a feasible method for voltage inversion in the line field; however, due to the interference of meteorological factors, this non-intrusive voltage measurement method has limitations in practical direct use. Therefore, it is also necessary to study the calibration method of humidity factor or the overall sealing protection of the measuring device. In future work, a non-intrusive line-voltage-measuring device can be developed by integrating a power module and a communication module with advanced micro-sensor technology.

Author Contributions: Conceptualization, Q.Y. and W.L.; methodology, Q.Y. and W.L.; validation, W.L. and Z.Q.; formal analysis, K.K. and Z.Q.; investigation, W.L. and K.K.; resources, Y.L. and F.J.; data curation, W.L. and Z.Q.; writing—original draft preparation, W.L. and K.K.; writing—review and editing, Q.Y.; supervision, Q.Y., Y.L. and F.J.; project administration, Y.L. and Q.Y.; funding acquisition, F.J. All authors have read and agreed to the published version of the manuscript.

Funding: This research was funded by the National Natural Science Foundations of China, grant number 52077019.

Data Availability Statement: Not applicable.

Conflicts of Interest: The authors declare no conflict of interest.

References

1. Strasser, T.; Andren, F.; Kathan, J.; Cecati, C.; Buccella, C.; Siano, P.; Leitao, P.; Zhabelova, G.; Vyatkin, V.; Vrba, P.; et al. A review of architectures and concepts for intelligence in future electric energy systems. *IEEE Trans. Ind. Electron.* **2015**, *62*, 2424–2438. [[CrossRef](#)]
2. Huang, A.Q.; Crow, M.L.; Heydt, G.T.; Zheng, J.P.; Dale, S.J. The future renewable electric energy delivery and management (FREEDM) system: The energy internet. *Proc. IEEE* **2010**, *99*, 133–148. [[CrossRef](#)]
3. Morello, R.; Mukhopadhyay, S.C.; Liu, Z.; Slomovitz, D.; Samantaray, S.R. Advances on sensing technologies for smart cities and power grids: A review. *IEEE Sens. J.* **2017**, *17*, 7596–7610. [[CrossRef](#)]
4. De La Cruz, J.; Gómez-Luna, E.; Ali, M.; Vasquez, J.C.; Guerrero, J.M. Fault location for distribution smart grids: Literature overview, challenges, solutions, and future trends. *Energies* **2023**, *16*, 2280. [[CrossRef](#)]

5. Zhang, W.; Yang, Y.; Zhao, J.; Huang, R.; Cheng, K.; He, M. Research on a non-contact multi-electrode voltage sensor and signal processing algorithm. *Sensors* **2022**, *22*, 8573. [[CrossRef](#)] [[PubMed](#)]
6. Zhang, W.; Wei, R.; Jiu, A.; Cheng, K.; Yang, Y.; Suo, C. Self-Calibration Method of Noncontact AC Voltage Measurement. *Electronics* **2023**, *12*, 300. [[CrossRef](#)]
7. Shenil, P.S.; George, B. Nonintrusive ac voltage measurement unit utilizing the capacitive coupling to the power system ground. *IEEE Trans. Instrum. Meas.* **2021**, *70*, 1–8. [[CrossRef](#)]
8. Xue, F.; Hu, J.; Guo, Y.; Han, G.; Ouyang, Y.; Wang, S.X.; He, J. Piezoelectric–piezoresistive coupling mems sensors for measurement of electric fields of broad bandwidth and large dynamic range. *IEEE Trans. Ind. Electron.* **2020**, *67*, 551–559. [[CrossRef](#)]
9. Li, J.; Liu, J.; Peng, C.; Liu, X.; Wu, Z.; Zheng, F. Design and Testing of a Non-Contact MEMS Voltage Sensor Based on Single-Crystal Silicon Piezoresistive Effect. *Micromachines* **2022**, *13*, 619. [[CrossRef](#)]
10. Luo, M.; Yang, Q.; Dong, F.; Chen, N.; Liao, W. Miniature micro-ring resonator sensor with electro-optic polymer cladding for wide-band electric field measurement. *J. Light. Technol.* **2022**, *40*, 2577–2584. [[CrossRef](#)]
11. Yang, Q.; Sun, S.; He, Y.; Han, R. Intense electric-field optical sensor for broad temperature-range applications based on a piecewise transfer function. *IEEE Trans. Ind. Electron.* **2019**, *66*, 1648–1656. [[CrossRef](#)]
12. Wang, J.; Gao, C.; Yang, J. Design, Experiments and Simulation of Voltage Transformers on the Basis of a Differential Input D-dot Sensor. *Sensors* **2014**, *14*, 12771–12783. [[CrossRef](#)]
13. Metwally, I.A. D-dot probe for fast-front high-voltage measurement. *IEEE Trans. Instrum. Meas.* **2010**, *59*, 2211–2219. [[CrossRef](#)]
14. Yang, P.; Wen, X.; Chu, Z.; Ni, X.; Peng, C. Non-intrusive DC voltage measurement based on resonant electric field microsensors. *J. Micromech. Microeng.* **2021**, *31*, 064001. [[CrossRef](#)]
15. Yang, P.; Wen, X.; Lv, Y.; Chu, Z.; Peng, C. A non-intrusive voltage measurement scheme based on MEMS electric field sensors: Theoretical analysis and experimental verification of AC power lines. *Rev. Sci. Instrum.* **2021**, *92*, 065002. [[CrossRef](#)]
16. Haberman, M.A.; Spinelli, E.M. A noncontact voltage measurement system for power-line voltage waveforms. *IEEE Trans. Instrum. Meas.* **2020**, *69*, 2790–2797. [[CrossRef](#)]
17. Sevlian, R.A.; Rajagopal, R. Actively calibrated line mountable capacitive voltage transducer for power systems applications. *IEEE Trans. Smart Grid* **2018**, *9*, 3942–3953. [[CrossRef](#)]
18. Han, Z.; Xue, F.; Hu, J.; He, J. Micro electric field sensors: Principles and applications. *IEEE Trans. Ind. Electron.* **2021**, *15*, 35–42. [[CrossRef](#)]
19. Kainz, A.; Steiner, H.; Schalko, J.; Jachimowicz, A.; Kohl, F.; Stifter, M.; Beigelbeck, R.; Keplinger, F.; Hortschitz, W. Distortion-free measurement of electric field strength with a MEMS sensor. *Nat. Electron.* **2018**, *1*, 68–73. [[CrossRef](#)] [[PubMed](#)]
20. Hu, G.; Li, P.; Liu, X.; Zhao, Y. Inverse source problems in electrodynamics. *Inverse Probl. Imaging* **2018**, *12*, 1411–1428. [[CrossRef](#)]
21. Xiao, D.; Xie, Y.; Liu, H.; Ma, Q.; Zheng, Q.; Zhan, Z. Position optimization of measuring points in voltage noncontact measurement of ac overhead transmission lines. *Appl. Comput. Electrom.* **2017**, *32*, 908–914.
22. Chavez, P.P.; Rahmatian, F.; Jaeger, N. Accurate voltage measurement with electric field sampling using permittivity-shielding. *IEEE Trans. Power Deliv.* **2002**, *17*, 362–368. [[CrossRef](#)]
23. Rahmatian, F.; Chavez, P.P.; Jaeger, N. 230 kV optical voltage transducers using multiple electric field sensors. *IEEE Trans. Power Deliv.* **2002**, *17*, 417–422. [[CrossRef](#)]
24. Chavez, P.P.; Jaeger, N.A.F.; Rahmatian, F. Accurate voltage measurement by the quadrature method. *IEEE Trans. Power Deliv.* **2003**, *18*, 14–19. [[CrossRef](#)]
25. Wang, J.; Li, X.; Wang, Q.; Zhong, L.; Zhu, X. Research on transmission line voltage measurement method based on Gauss-Kronrod integral algorithm. *Meas. Sci. Technol.* **2020**, *31*, 85103. [[CrossRef](#)]
26. Wang, J.; Yan, X.; Li, X.; Liao, J.; Tao, Y. Method and experimental study of transmission line voltage measurement based on a gauss-type integral algorithm. *Trans. China Electrotech. Soc.* **2021**, *36*, 3978–3986. (In Chinese)
27. Wen, X.; Yang, P.; Chu, Z.; Peng, C.; Liu, Y.; Wu, S. Toward Atmospheric Electricity Research: A Low-Cost, Highly Sensitive and Robust Balloon-Borne Electric Field Sounding Sensor. *IEEE Sens. J.* **2021**, *21*, 13405–13416. [[CrossRef](#)]

Disclaimer/Publisher’s Note: The statements, opinions and data contained in all publications are solely those of the individual author(s) and contributor(s) and not of MDPI and/or the editor(s). MDPI and/or the editor(s) disclaim responsibility for any injury to people or property resulting from any ideas, methods, instructions or products referred to in the content.